JACS
JOURNAL OF THE AMERICAN CHEMICAL SOCIETY
Communication
pubs.acs.org/JACS

Ultrasound-Modulated Bubble Propulsion of Chemically Powered Microengines

Tailin Xu,[†,‡,§] Fernando Soto,[†,§] Wei Gao,[†] Victor Garcia-Gradilla,[†] Jinxing Li,[†] Xueji Zhang,[‡] and Joseph Wang*[,†]

[†]Departments of Nanoengineering and Engineering, University of California—San Diego, La Jolla, California 92093, United States
[‡]Research Center for Bioengineering and Sensing Technology, University of Science and Technology Beijing, Beijing 100083, P. R. China

Supporting Information

ABSTRACT: The use of an ultrasound (US) field for rapid and reversible control of the movement of bubble-propelled chemically powered PEDOT/Ni/Pt microengines is demonstrated. Such operation reflects the US-induced disruption of normal bubble evolution and ejection, essential for efficient propulsion of catalytic microtubular engines. It offers precise speed control, with sharp increases and decreases of the speed at low and high US powers, respectively. A wide range of speeds can thus be generated by tuning the US power. Extremely fast changes in the motor speed (<0.1 s) and reproducible "On/Off" activations are observed, indicating distinct advantages compared to motion control methods based on other external stimuli. Such effective control of the propulsion of chemically powered microengines, including remarkable "braking" ability, holds considerable promise for diverse applications.

Chemically powered nano-/microscale motors have received considerable recent attention.[1−12] In particular, bubble-propelled catalytic tubular microengines have shown promise for many important biomedical and environmental applications.[13−20] The ability of such microengines to perform complex operations requires a precise control of their motion. Control of the directionality of catalytic micromotors has been commonly achieved by means of magnetic fields.[21−27] Various strategies have been employed to regulate the speed of such micromotors, including application of thermal,[28−31] optical,[32,33] or electrical[34] stimuli, control of motor composition,[35] and control of microchip structures.[36]

Here we demonstrate precise, rapid, and reversible control of the speed of bubble-propelled chemically powered microengines through application of ultrasound (US) fields. Ultrasound is widely used for biomedical applications[37−39] and has the capability to cavitate, coalesce, and collapse gas bubbles.[40−42] Taking advantage of the effect of US upon gas bubbles, we demonstrate herein the use of an US field to regulate and modulate the speed of catalytic microengines. This operation relies on the large translational movement of the coalesced bubbles and the significant growth and aggregation of microbubbles in the presence of an US field, a process that hinders the regular bubble evolution on the larger opening of the microtubular engine. Unlike the long response times of speed-controlled approaches—based on thermal or optical stimuli—that affect the fuel level or reaction rate (and indirectly the bubble formation),[29,32] the tubular microengines respond nearly instantaneously (within 0.1 s) to the US field owing to its direct effect upon the bubble evolution and ejection. This reversible and rapid US motion control represents an effective approach for regulating on demand the operation of catalytic microengines.

As illustrated in Figure 1, US-based control of the movement of catalytic microengines results from the effect of the US field upon the evolution of the generated oxygen microbubbles. The bubble-propulsion mechanism of tubular microengines has been described previously.[43,44] The propulsion thrust reflects the release of individual oxygen microbubbles, generated on the inner Pt surface by the catalytic decomposition of the hydrogen peroxide fuel. The ejection of the microbubbles from the wider opening of the microtubes thus leads to discrete step-by-step displacements of the motor (Figure 1, left). The propulsion thrust generated by the momentum associated with the ejection of the individual bubbles results a linear motion of the microengine.[43] Application of an US field disrupts the bubble evolution and hinders the movement (Figure 1, right). Video S1 provides a direct observation of the bubble evolution and

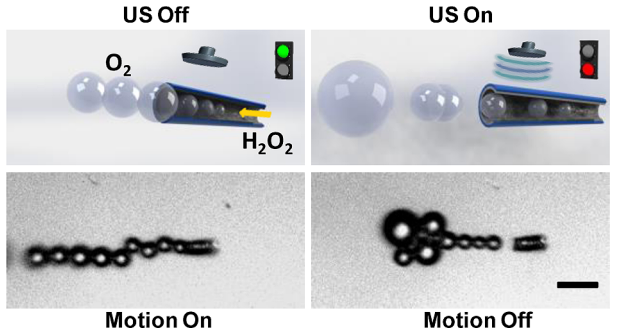

Figure 1. Schematic (top) and microscope images (bottom) of the ultrasound-based modulated motion of a chemically powered PEDOT/Ni/Pt microengine. The presence of an US field disrupts the bubble evolution at the larger opening of the microengines, resulting in greatly diminished propulsion. Scale bar, 20 μm.

Received: April 25, 2014
Published: June 4, 2014

dx.doi.org/10.1021/ja504150e | J. Am. Chem. Soc. 2014, 136, 8552−8555

ejection behavior and a clear illustration of the new US-induced "braking" ability of the chemically powered microengines.

Previous reports showed that the interference between different standing acoustic waves establishes a differential pressure field in the fluid; acoustic radiation forces result from pressure gradients in the incident and scattered ultrasonic fields that drive gas bubbles to nodes or anti-nodes in the acoustic pressure field.[45] The acoustic radiation forces on gas bubbles are normally referred to as Bjerknes forces. These forces are normally divided into two basic types: primary Bjerknes forces (F_1) and secondary Bjerknes forces (F_2). The primary Bjerknes forces, experienced by single bubbles and causing bubbles to migrate in an acoustic field or to gather in certain areas (e.g., pressure nodes), can be expressed as[46]

$$F_1 = \frac{2\pi |A_m|^2 \delta R_0 \kappa}{\rho_0 \omega^2 [(1 - \omega_0^2/\omega^2)^2 + \delta^2]} \quad (1)$$

where ρ_0 is the equilibrium liquid density, ω_0 is the resonance angular frequency of the bubble, ω is the driving acoustic angular frequency (1.0 MHz), δ is the total damping constant, A_m is the complex pressure amplitude which is proportional to applied transducer potential, and κ is the wave vector in the liquid. The secondary Bjerknes forces, responsible for the bubble interactions, which lead to the attraction of individual bubbles, are given by[46]

$$F_2 = \frac{2\pi R_{10} R_{20} |A_m|^2 [(1 - \omega_1^2/\omega^2)(1 - \omega_2^2/\omega^2) + \delta_1 \delta_2]}{\rho_0 \omega^2 L^2 [(1 - \omega_1^2/\omega^2)^2 + \delta_1^2][(1 - \omega_2^2/\omega^2)^2 + \delta_2^2]} \quad (2)$$

where R_{10} and R_{20} are the equilibrium radii, which are dependent on the size of the microengines ($R_{10} = R_{20}$ for the same engine), ω_1 and ω_2 are resonance angular frequencies of the bubbles, δ_1 and δ_2 are their total damping constants, and L is the distance between two bubbles. Considering that $\omega_1 = \omega_2$ and $\delta_1 = \delta_2$ for bubbles generated from the same engine, F_2 is always larger than zero, which means that bubbles attract each other. Detailed mathematical discussions of these two forces are provided in Supporting Information. When an US field is applied on a moving microtubular engine, oxygen bubbles—generated inside the tube—are ejected immediately from the microtube (without a normal gradual growth) due to the primary Bjerknes forces and rapidly aggregate to form large bubbles due to secondary Bjerknes forces (Figure 1, right). The combined effect of these two forces disrupts the normal bubble evolution and ejection at the larger opening of the microengines (Figure 1, right), which is critical for efficient propulsion. Such changes in the normal bubble evolution of the microengines result in a greatly diminished propulsion. Careful examination of the videos indicates that the microengines sometimes recoil back very slightly under the US field. This may be attributed to the flow generated from the bubble translational motion and aggregation. In contrast, the microengines remain static under the US field in the absence of hydrogen peroxide fuel.

Reversibly and rapidly stopping and starting artificial micromotors is commonly a major technological challenge. Figure 2 and corresponding Video S2 illustrate the reversible and rapid "Stop−Go" switching of the microengine motion upon applying repetitive US field. A catalytic poly(3,4-ethylenedioxythiophene) (PEDOT)/Ni/Pt tubular microengines (15 μm long, 5 μm diameter in the wider side) fabricated by the template electrodeposition[47] (see Supporting Information for experimental details). In the absence of the US field, the microengine moves normally, with a characteristic bubble tail, at a high velocity of 231 μm/s. Application of the US field (10 V of US transducer voltage) results in a remarkable "braking" ability (within 0.1 s; Figure S1). As a result, the microengine stops its movement nearly completely after application of the US field, keeping only a negligible velocity of 6 μm/s. The microengine rapidly resumes its movement after the US field is been turned off, regaining its original speed within 0.1 s. Such multiple 1-s "Stop−Go" maneuvers, i.e., cyclic "On/Off" US activations, illustrate the reversibility of US-based motion control. The cyclic "On/Off" US activation of the nanomotor motion can be repeated several times. Unlike earlier motion-control methods—based on thermal, optical, or electrical stimuli—which modulate the propulsion by controlling the fuel level or reaction rate,[28−32] the US-based speed control directly affects the bubble evolution and thus results in extremely fast response times. The speed/US-power temporal profiles in Figure 2 indicate great promise for regulating on demand the motion of catalytic microengines in connection to an external "On/Off" US switch.

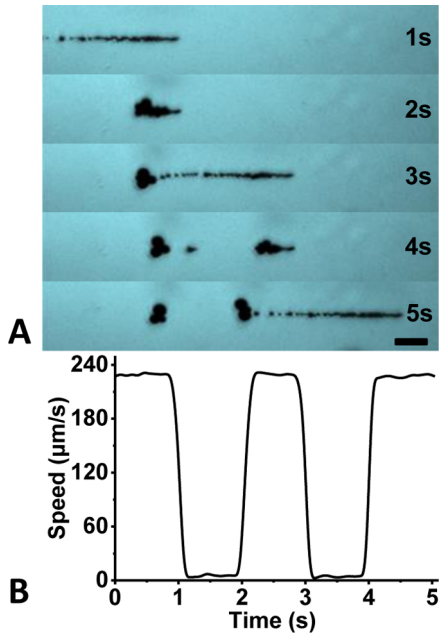

Figure 2. Cyclic "On" and "Off" ultrasound activation of the PEDOT/Ni/Pt microengine motion. Time-lapse images (A) and corresponding speed/time dependence (B) illustrating the US-triggered "On/Off" motion control of the PEDOT/Ni/Pt microengine in a 2% H_2O_2 solution containing 5% NaCh. The microscopic images were taken at 1-s intervals from Video S2. Scale bar, 50 μm. Ultrasound field: 10 V, 1 MHz.

The extent of bubble disruption, and hence the speed diminution, depends upon the power of the applied US field, which is controlled by the applied transducer voltage. The pressure produced by the US field, which has a direct influence on the Bjerknes forces, is directly proportional to the voltage amplitude at a given frequency (see eqs 1 and 2). As a result, a wide range of microengine speeds can be generated (using the same fuel level) via fine control of the US field. Such precise speed control is illustrated in Figure 3 and corresponding Video S3. For example, the observed motion trajectories of the microengine, taken from Video S3, illustrate the precisely regulated velocity using a variety of US amplitudes,

dx.doi.org/10.1021/ja504150e | J. Am. Chem. Soc. 2014, 136, 8552−8555

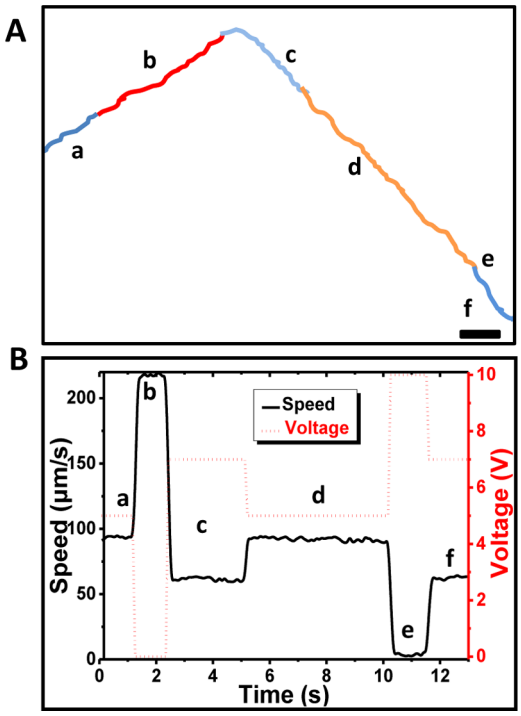

Figure 3. Ultrasound-triggered speed modulation of catalytic microengines upon switching the US transducer voltage to 5 V (a), 0 V (b), 7 V (c), 5 V (d), 10 V (e), and 7 V (f). (A) Motion trajectories taken from Video S3. Scale bar, 50 μm. (B) Speed modulation of the microengines (black) in connection to the different voltages (red). Other conditions as in Figure 2.

corresponding to different transducer voltages (a, 5 V; b, 0 V; c, 7 V; d, 5 V; e, 10 V; and f, 7 V) over different time intervals. Such changes in the US power lead to real-time speed modulation of the microengines, with sharp increases and decreases of the speed at low and high voltages, respectively: 217.2, 93.4, 61.4, and 3.7 μm/s at 0, 5, 7, and 10 V, respectively. These data clearly demonstrate the complete reversibility of the US-triggered speed modulation (with response times nearly independent of the US voltage) and that the microengine rapidly accelerates and decelerates upon application of different transducer voltages. A wide range of speeds can thus be generated through fine control of the US power. Such an effect of different US amplitudes is attributed to the different rates of bubble aggregation under different US fields, reflecting the dependence of the applied amplitudes on the Bejerkns forces (Supporting Information eqs 3 and 5). Higher US powers lead to higher Bejerkns forces and thus to a faster bubble immigration and aggregation process, which leads to further deceleration on the microengines.

The speed of the bubble-driven PEDOT/Ni/Pt microengines is strongly dependent on the concentration of hydrogen peroxide, which influences the radius and frequency of the generated oxygen bubbles.[47] Accordingly, it is essential to assess the efficiency of the US-based speed regulation in the presence of different fuel levels, and particularly the influence of the initial motor speed upon the US "braking" ability. Figure 4 illustrates the US-modulated speed of catalytic PEDOT/Ni/Pt microtube engines in four different concentrations of hydrogen peroxide: 0.5%, 1%, 2%, and 5%. The initial average speeds of the microengines are 24 ± 5, 88 ± 25, 231 ± 30, and 696 ± 61 μm/s in the presence of 0.5%, 1%, 2%, and 5% hydrogen

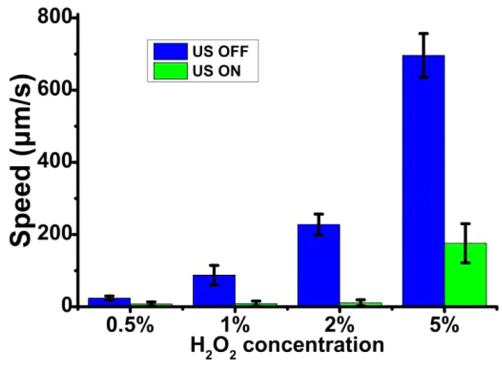

Figure 4. Ultrasound-modulated speed of catalytic microengines in the presence of different fuel concentrations. Other conditions as in Figure 2.

peroxide, respectively. When the US field was turned "On" (10 V, 1 MHz), the microengine motion stopped immediately in the 0.5%, 1%, and 2% hydrogen peroxide solutions, reaching negligible speeds of 7 ± 5, 8 ± 6, and 10 ± 8 μm/s, respectively. Apparently, the microengine retains its remarkable US-based braking capability at these different fuel levels. However, for the extremely fast propulsion (e.g., 696 ± 61 μm/s using an elevated 5% hydrogen peroxide concentration), the speed was greatly reduced to 175 ± 54 μm/s (see Video S4). Complete stoppage of the microengine motion at this high fuel level would require the use of higher US powers (i.e., stronger "brakes"). The presence of a surfactant (sodium cholate in this work) is essential to the new operation, in view of its key role in the bubble evolution.

In conclusion, we have demonstrated that ultrasound stimuli can be used for regulating the movement of chemically powered tubular microengines. Such rapid and reversible motion control, including instantaneous "On/Off" activations, is attributed to the direct effect of the US field upon the evolution of the generated oxygen microbubbles. The extremely fast changes in the motor speed represent a distinct advantage compared to other motion control methods. The new speed modulation capability can be expanded to other types of bubble-propelled micromotors.[48−50] Preliminary results in this direction are very encourging (not shown). This ability to use ultrasound to trigger the motion of tubular microengines and to regulate their speed offers an elegant route for controlling the operation of catalytic microengines and holds considerable promise for challenging new applications of these nano-/microscale motors.

■ ASSOCIATED CONTENT

Supporting Information

Experimental details, microengines preparation, US equipment, detailed mathematical discussions, reagents, additional figures, and videos S1−S4. This material is available free of charge via the Internet at http://pubs.acs.org.

■ AUTHOR INFORMATION

Corresponding Author

josephwang@ucsd.edu

Author Contributions

[§]T.X. and F.S. contributed equally to this paper.

Notes

The authors declare no competing financial interest.

■ ACKNOWLEDGMENTS

This project received support from the Defense Threat Reduction Agency-Joint Science and Technology Office for Chemical and Biological Defense (Grant No. HDTRA1-13-1-0002). T.X. acknowledges the China Scholarship Council (CSC) for financial support. W.G. is a HHMI International Student Research fellow. The authors thank Guoqing Pan and Michael Galarnyk for their help in the microengines preparation.

■ REFERENCES

(1) Paxton, W. F.; Kistler, K. C.; Olmeda, C. C.; Sen, A.; St. Angelo, S. K.; Cao, Y.; Mallouk, T. E.; Lammert, P. E.; Crespi, V. H. *J. Am. Chem. Soc.* **2004**, *126*, 13424−13431.
(2) Ozin, G. A.; Manners, I.; Fournier-Bidoz, S.; Arsenault, A. *Adv. Mater.* **2005**, *17*, 3011.
(3) Fournier-Bidoz, S.; Arsenault, A. C.; Manners, I.; Ozin, G. A. *Chem. Commun.* **2005**, *4*, 441−443.
(4) Kline, T. R.; Paxton, W. F.; Mallouk, T. E.; Sen, A. *Angew. Chem., Int. Ed.* **2005**, *44*, 744−746.
(5) Wang, J. *Nanomachines: Fundamentals and Applications*; John Wiley & Sons: Weinheim, 2013.
(6) Mirkovic, T.; Zacharia, N. S.; Scholes, G. D.; Ozin, G. A. *ACS Nano* **2010**, *4*, 1782.
(7) Mallouk, T. E.; Sen, A. *Sci. Am.* **2009**, *300*, 72.
(8) Mei, Y.; Solovev, A. A.; Sanchez, S.; Schmidt, O. G. *Chem. Soc. Rev.* **2011**, *40*, 2109.
(9) Wang, J.; Gao, W. *ACS Nano* **2012**, *6*, 5745.
(10) Ebbens, S. J.; Howse, J. R. *Soft Matter* **2010**, *6*, 726.
(11) Sanchez, S.; Pumera, M. *Chem.—Asian J.* **2009**, *4*, 1402.
(12) Wang, W.; Duan, W.; Ahmed, S.; Mallouk, T. E.; Sen, A. *Nano Today* **2013**, *8*, 531.
(13) Solovev, A. A.; Mei, Y.; Bermudez Urena, E.; Huang, G.; Schmidt, O. G. *Small* **2009**, *5*, 1688.
(14) Huang, G.; Wang, J.; Mei, Y. *J. Mater. Chem.* **2012**, *22*, 6519.
(15) Campuzano, S.; Orozco, J.; Kagan, D.; Guix, M.; Gao, W.; Sattayasamitsathit, S.; Claussen, J. C.; Merkoci, A.; Wang, J. *Nano Lett.* **2012**, *12*, 396.
(16) Solovev, A. A.; Xi, W.; Gracias, D. H.; Harazim, S. M.; Deneke, C.; Sanchez, S.; Schmidt, O. G. *ACS Nano* **2012**, *6*, 1751.
(17) Gao, W.; Wang, J. *ACS Nano* **2014**, *8*, 3170.
(18) Guix, M.; Orozco, J.; Garcia, M.; Gao, W.; Sattayasamitsathit, S.; Merkoci, A.; Escarpa, A.; Wang, J. *ACS Nano* **2012**, *6*, 4445.
(19) Soler, L.; Magdanz, V.; Fomin, V. M.; Sanchez, S.; Schmidt, O. G. *ACS Nano* **2013**, *7*, 9611.
(20) Soler, L.; Sanchez, S. *Nanoscale* **2014**, DOI: 10.1039/C4NR01321B.
(21) Wang, J.; Manesh, K. M. *Small* **2010**, *6*, 338.
(22) Burdick, J.; Laocharoensuk, R.; Wheat, P. M.; Posner, J. D.; Wang, J. *J. Am. Chem. Soc.* **2008**, *130*, 8164.
(23) Solovev, A. A.; Sanchez, S.; Pumera, M.; Mei, Y. F.; Schmidt, O. G. *Adv. Funct. Mater.* **2010**, *20*, 2430.
(24) Fischer, P.; Ghosh, A. *Nanoscale* **2011**, *3*, 557.
(25) Khalil, I. S.; Magdanz, V.; Sanchez, S.; Schmidt, O. G.; Misra, S. *PLoS One* **2014**, *9*, e83053.
(26) Zhao, G.; Pumera, M. *Langmuir* **2013**, *29*, 7411.
(27) Zhao, G.; Sanchez, S.; Schmidt, O. G.; Pumera, M. *Chem. Commun.* **2012**, *48*, 10090.
(28) Balasubramanian, S.; Kagan, D.; Manesh, K. M.; Calvo-Marzal, P.; Flechsig, G. U.; Wang, J. *Small* **2009**, *5*, 1569.
(29) Sanchez, S.; Ananth, A. N.; Fomin, V. M.; Viehrig, M.; Schmidt, O. G. *J. Am. Chem. Soc.* **2011**, *133*, 14860.
(30) Gao, W.; Sattayasamitsathit, S.; Wang, J. *Chem. Rec.* **2012**, *12*, 224.
(31) Magdanz, V.; Stoychev, G.; Ionov, L.; Sanchez, S.; Schmidt, O. G. *Angew. Chem., Int. Ed.* **2014**, *53*, 2673.
(32) Solovev, A. A.; Smith, E. J.; Bof' Bufon, C. C.; Sanchez, S.; Schmidt, O. G. *Angew. Chem., Int. Ed.* **2011**, *50*, 10875.
(33) Liu, Z.; Li, J.; Wang, J.; Huang, G.; Liu, R.; Mei, Y. *Nanoscale* **2013**, *5*, 1345.
(34) Calvo-Marzal, P.; Manesh, K. M.; Kagan, D.; Balasubramanian, S.; Cardona, M.; Flechsig, G. U.; Posner, J.; Wang, J. *Chem. Commun.* **2009**, 4509.
(35) Gao, W.; Sattayasamitsathit, S.; Uygun, A.; Pei, A.; Ponedal, A.; Wang, J. *Nanoscale* **2012**, *4*, 2447.
(36) Restrepo-Perez, L.; Soler, L.; Martinez-Cisneros, C.; Sanchez, S.; Schmidt, O. G. *Lab Chip* **2014**, *14*, 1515.
(37) Olson, E. S.; Orozco, J.; Wu, Z.; Malone, C. D.; Yi, B.; Gao, W.; Eghtedari, M.; Wang, J.; Mattrey, R. F. *Biomaterials* **2013**, *34*, 8918.
(38) Mitragotri, S. *Nat. Rev. Drug Discovery* **2005**, *4*, 255.
(39) Marmottant, P.; Hilgenfeldt, S. *Nature* **2003**, *423*, 153.
(40) Stride, E. P.; Coussios, C. C. *Proc. Inst. Mech. Eng. H* **2010**, *224*, 171.
(41) Postema, M.; van Wamel, A.; Lancee, C. T.; de Jong, N. *Ultrasound Med. Biol.* **2004**, *30*, 827.
(42) Fan, Z.; Chen, D.; Deng, C. X. *Ultrasound Med. Biol.* **2014**, *40*, 1260.
(43) Li, J.; Huang, G.; Ye, M.; Li, M.; Liu, R.; Mei, Y. *Nanoscale* **2011**, *3*, 5083.
(44) Manjare, M.; Yang, B.; Zhao, Y. P. *J. Phys. Chem. C* **2013**, *117*, 4657.
(45) Woodside, S. M.; Bowen, B. D.; Piret, J. M. *AIChE J.* **1997**, *43*, 1727.
(46) Doinikov, A. A. *Bubble and Particle Dynamics in Acoustic Fields: Modern Trends and Applications*; Research Signpost: Kerala, India, 2005.
(47) Gao, W.; Sattayasamitsathit, S.; Orozco, J.; Wang, J. *J. Am. Chem. Soc.* **2011**, *133*, 11862.
(48) Gao, W.; D'Agostino, M.; Garcia-Gradilla, V.; Orozco, J.; Wang, J. *Small* **2013**, *9*, 467.
(49) Wang, H.; Zhao, G.; Pumera, M. *J. Am. Chem. Soc.* **2014**, *136*, 2719.
(50) Gao, W.; Pei, A.; Wang, J. *ACS Nano* **2012**, *6*, 8432.